Progress In Electromagnetics Research, Vol. 122, 93–103, 2012

MATRIX STRUCTURE OF METAMATERIAL ABSORBERS FOR MULTISPECTRAL TERAHERTZ IMAGING

S. A. Kuznetsov[1, 2], A. G. Paulish[1, 3, *], A. V. Gelfand[3], P. A. Lazorskiy[3], and V. N. Fedorinin[3]

[1]Novosibirsk State University, Pirogova St., 2, Novosibirsk 630090, Russian Federation

[2]Budker Institute of Nuclear Physics SB RAS National Institute, Lavrentiev Ave., Novosibirsk 630090, Russian Federation

[3]Institute of Semiconductor Physics SB RAS, Novosibirsk Branch "TDIAM", Lavrentiev Ave., 2/1, Novosibirsk 630090, Russian Federation

Abstract—A multispectral 24 × 24 bolometric matrix structure of terahertz (THz) absorbers operating at 0.3–0.4 THz was proposed and experimentally investigated. Each pixel of the structure was implemented as a fragment of an ultra-thin metamaterial absorber. The matrix structure consisted of four types of pixels with nearly perfect absorptivity. Three pixels were at 0.30, 0.33, 0.36 THz respectively with identically oriented polarization sensitivity, and the fourth pixel was at 0.33 THz oriented with polarization sensitivity orthogonal to foregoing ones. The backside of the structure included a high-performance infrared emissive layer. Resonant absorption of THz radiation induced the structure heating and increasing IR emission from the emissive layer, which was henceforth detected by the IR camera. The terahertz imaging system, capable to operate in real time, with spectral and polarization discrimination was demonstrated. The experimental results showed good spectral and polarization resolution together with acceptable spatial resolution.

1. INTRODUCTION

Multispectral and hyperspectral imaging are powerful techniques, which expand informativity of the inspected objects by detecting

Received 14 October 2011, Accepted 7 November 2011, Scheduled 15 November 2011

* Corresponding author: Andrey Georgievich Paulish (paulish63@ngs.ru).

images simultaneously in tens or hundreds spectral bands [1–3]. Such an approach to enhance discrimination between different types of investigated objects or materials is commonly used in the visible and infrared ranges, and is effectively utilized for remote sensing in mineralogy, agriculture, geology and biomedical engineering [1–8].

Multispectral imaging has the same prospects for the rapidly developing terahertz science and technology [9–20]. The use of terahertz waves to spectroscopically detect and identify concealed materials through their characteristic transmission or reflection spectra is one of the prospective solutions for locating, detecting and characterizing concealed threats such as plastic explosives, chemical and biological agents, illegal drugs [12–14]. For example, many explosives (such as C-4, HMX, RDX and TNT) and illegal drugs (for example, methamphetamine) have characteristic transmission/reflection spectra in the THz range that could be distinguishable from other materials such as clothing, wrappers and human skin. These materials should appear in different 'colors' to a THz detector as compared to non-hazardous items. Using THz spectroscopy, it should be possible to detect explosives or drugs even if they are concealed, since the THz radiation is readily transmitted through plastics, clothing, paper products and other non-conductive (non-metallic) materials. By comparing measured THz spectra with known calibration spectra (spectral fingerprints), one may identify the presence of these agents and distinguish them from benign objects. The multispectral THz imaging has the same prospects for the investigation of biomedical tissues, such as probing surface and subcutaneous properties of skin and detection of tooth decay [16–19]. In [14, 15, 17, 18], the frequency sweep together with 2D scanning was used for multispectral image processing. The main disadvantage of the described methods was in long time procedure of sequential sample scanning at different frequencies. A multispectral imaging system for millimeter wavelengths based on cascade of matrix absorbers was proposed in [21] for space researches. But this system operated at cryogenic temperatures. However, for ground-based sensing, it is desirable to create an uncooled, inexpensive and easy-to-use system, capable of operating in real time.

2. MULTISPECTRAL TERAHERTZ-TO-INFRARED CONVERTER

2.1. Pixel Structure

In a previous work [22], we proposed an uncooled terahertz imaging system operating in real time. The system was designed for operation

at a single frequency of 0.30 THz and utilized the scheme of terahertz (THz) to infrared (IR) conversion with IR detection by a conventional IR camera. Using this approach, in this work we proposed a multispectral terahertz sensor which had a 24×24 focal plane array of polarization-selective resonant absorbers (pixels) operating at 0.30, 0.33, 0.36 THz (Fig. 1). Each pixel of the array was implemented as a $0.9 \times 0.9\,\mathrm{mm}^2$ unit of an ultra-thin artificial impedance surface [23] (AIS). The pixel size was chosen to be close to operational wavelength in order to minimize the overall dimension of the structure. The pixels were located on the square lattice with X- and Y-periodicities of 1.3 mm. Each AIS unit included a subwavelength frequency-selective surface (FSS) or metasurface (MS), and a dielectric film with metal "ground" layer (Fig. 1). The free-space wavelength exceeded the AIS thickness by a factor of 41–50. Such optically thin absorbers were considered as a kind of metamaterial structures [24, 25].

A graphitized layer of 10 µm deposited over the outer surface of the AIS layer, served as an infrared emissive layer with nearly perfect absorptivity (emissivity factor of 0.93). Resonant absorption of THz

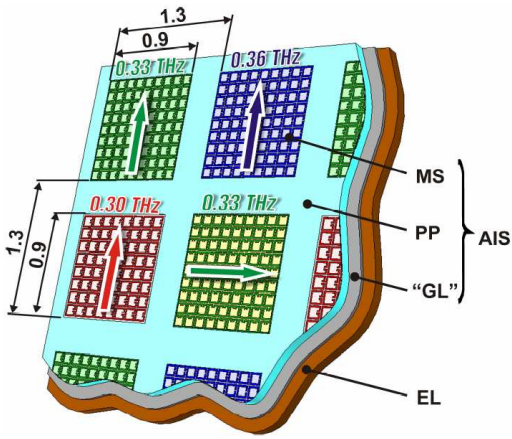

Figure 1. Scheme of matrix structure of the absorbers. AIS — artificial impedance surface, which acts as a metamaterial absorber and includes: MS — metasurface, PP — polypropylene film, "GL" — metal "ground" layer. Resonant frequencies, size and period (in millimeters) of the pixels are indicated in the figure. Arrows indicate the direction of the linear polarization corresponding to the maximal absorption. EL — IR emissive layer. Thicknesses of the PP film and EL are 20 and 10 µm, respectively. Thickness of the aluminum layer for MS and "GL" is 0.4 µm.

radiation induced the sufficient pixel heating that increased an infrared radiation emission from the emissive layer. The IR emission was detected by a commercial IR camera.

2.2. Converter Fabrication

A polypropylene film (PP) with a thickness $d = 20\,\mu m$ was used as the AIS dielectric self-supporting substrate. The PP film was metallized on both sides by a thermal vacuum deposition of $0.4\,\mu m$ thick aluminum as the highly-conductive "ground" back and top layers. A photolithographically-patterned split ring resonator array (SRR) [22, 26, 27] was utilized as a polarization-selective metasurface of a capacitive type in the AIS with a configuration of "metasurface + grounded dielectric slab" (Fig. 2).

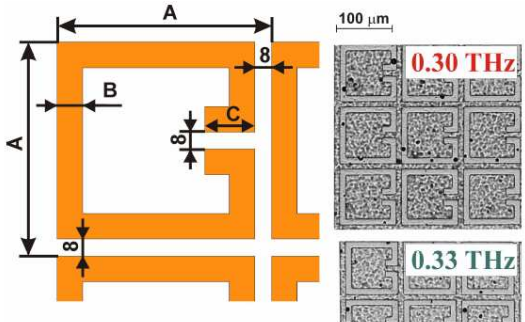

THz	A	B	C
0.30	110	12	27.5
0.33	102.8	12.2	24
0.36	100.5	14.3	14.9

Figure 2. (left) Scheme and geometric parameters (in micrometers) of split-ring resonators optimized for absorption at 0.30, 0.33, 0.36 THz. (right) Photomicrographs of the topological pattern of fabricated split-ring resonators.

2.3. SRR Parameters

The SRR geometric parameters of each THz absorber were numerically optimized by a 3D Full-wave electromagnetic analysis using the Ansoft HFSS^{TM} software by exploiting the regime of Floquet ports and periodic boundary conditions applied to the AIS unit cell. For a fixed PP thickness of 20 µm, an optimal combination of SRR geometric parameters (A, B, C in Fig. 2(a)) were determined to provide a reflectivity factor below −30 dB at AIS resonance frequencies ν = 0.30, 0.33, 0.36 THz. Photomicrographs of the fabricated split-ring resonators are shown in Fig. 2(b). The absorption spectra, derived from the simulated and experimentally measured reflectivity spectra related to the normal excitation, are shown in Fig. 3. The upper and lower spectra correspond to co-polar (**E** ⊥ SRR gaps) and

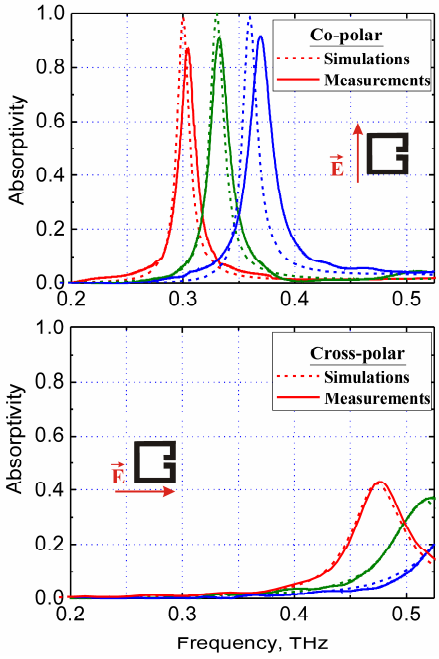

Figure 3. Absorptivity spectra of the absorbers for two orthogonal polarizations. Simulated and measured spectra are shown by dashed and solid lines respectively. Polarization directions relative to SRR gap for co-polar (**E** ⊥ SRR gaps) and cross-polar (**E** ∥ SRR gaps) polarization modes are shown in insets.

cross-polar (**E** ∥ SRR gaps) polarization modes respectively, where **E** is the vector of the electric field. A good agreement between simulations and measurements can be seen from the figure. The relative bandwidth $\Delta\nu/\nu$ of the co-polar absorption resonance is 6% at out-of-band absorptivity below 2% up to 0.55 THz. This provides a high spectral selectivity of the sensor. The second-order resonance for co-polar excitation appears only at frequencies above 0.70 THz. For cross-polar excitation, the absorption resonance is shifted towards higher frequencies approximately by 60% relative to the fundamental resonance at co-polar excitation. It is essential that the cross-polar absorptivity at the resonant frequency of co-polar excitation (0.30, 0.33, 0.36 THz) is below 2% that provides a high polarization discrimination of the proposed absorber.

2.4. Matrix Structure

The matrix structure consists of four types of the absorbers described above (Fig. 1). Three absorbers with resonant frequencies at 0.30, 0.33, 0.36 THz have identical polarization sensitivity (shown by arrows). The fourth absorber with a resonant frequency at 0.33 THz has a polarization sensitivity orthogonal to foregoing ones due to a 90-degree turn of the topological pattern in this array. Hence, the polarization direction of the incident linear polarized radiation at 0.33 THz can be determined by comparing signal intensities of orthogonally oriented pixels. Polarization difference imaging technique can facilitate detection and feature extraction of targets in scattering or reflecting media (see, for example, works [28–31] and references there).

3. EXPERIMENTAL SETUP

The proposed matrix structure was fabricated and experimentally investigated using a backward wave oscillator (BWO) with tunable output wavelength and 3–10 mW emission power as the source of monochromatic terahertz radiation both for imaging experiments and AIS characterization. The optical scheme for imaging experiments is shown in Fig. 4. The matrix structure was illuminated by a terahertz beam from the metasurface side, while IR radiation from the emissive layer was detected by the IR camera. We used IR camera with Noise Equivalent Temperature Difference (NETD) of 0.1 K. To reduce the energy dissipation due to an air thermal conductivity, the structure was placed into a vacuum chamber, which is supplied with input THz window (high density polyethylene) and with output IR window (coated ZnSe). To reduce a lateral thermal conductivity

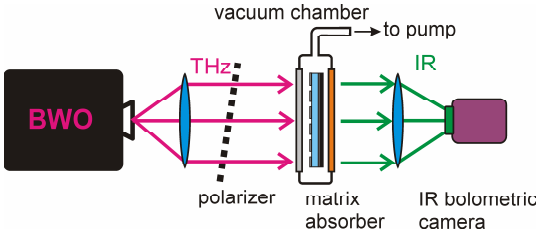

Figure 4. Optical scheme for imaging experiments. BWO — backward wave oscillator, vacuum chamber is supplied with input THz window (high density polyethylene) and with output IR window (coated ZnSe).

through the structure, the metal "ground" layer and emissive layer between metasurface fragments (pixels) were removed by the explosive photolithography.

4. EXPERIMENTAL RESULTS

We consecutively measured the images at BWO frequencies, 0.30 THz (4.0 mW), 0.33 THz (3.1 mW) and 0.36 THz (2.8 mW), under co-polar excitation for each type of pixels (Fig. 5, top). Each type of pixel is colored for better perception of the matrix image. The red, green and blue colors indicate the pixels with resonant absorptivity at 0.30, 0.33, and 0.36 THz, respectively and correspond to identical ("vertical") polarization sensitivity. The yellow color corresponds to pixels with resonant absorptivity at 0.33 THz, but with polarization sensitivity oriented orthogonally ("horizontally") to the previous three.

Arrows in Fig. 5 indicate the direction of the linear polarization corresponding to the maximal absorption. The image composed of four consecutively received monochromatic images is shown in Fig. 5 (bottom). It can be seen that signals from pixels produce good spatial resolution. The compound image, shown in Fig. 5, will be real in case of using a nonpolarized broadband source of radiation, containing frequencies within a range of 0.3–0.4 THz. As shown in our previous work [22], such a converter provides detection of THz radiation in real time due to small thickness of the converter and, therefore, its small thermal capacity. Unlike the multispectral imaging systems described in [14, 15, 17, 18], our approach allows simultaneous multispectral imaging with a desired set of frequencies. Such a multichannel receiver improves the efficiency of the measurements.

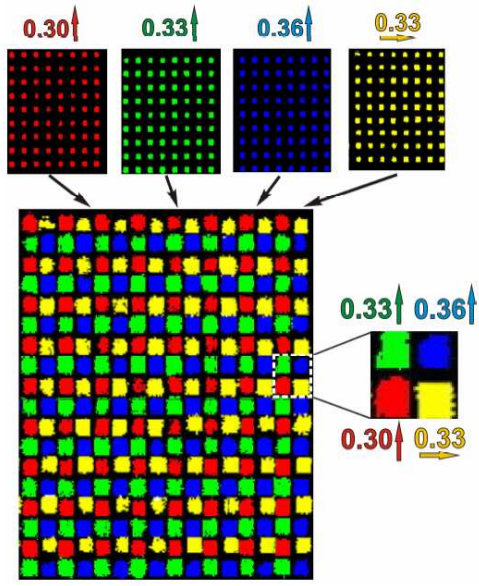

Figure 5. Fragment of image of the matrix structure (bottom), which is composed of four consecutively received IR images under monochromatic terahertz illumination from a BWO (top). Red, green, and blue spots correspond respectively to pixels with resonant absorption frequencies, 0.30, 0.33, and 0.36 THz and "vertical" polarization sensitivity (shown by arrows). The yellow spots indicate pixels with resonant absorption frequency (0.33 THz) and sensitive to "horizontal" polarization (shown by yellow arrows). This matrix unit cell is magnified at right.

5. CONCLUSION

We proposed and realized a multispectral 24 × 24 bolometric matrix structure for multi-spectral terahertz imaging with polarization resolution. The structure utilized the principle of terahertz to infrared conversion. Each cell of the structure was represented as a single fragment of an ultra-thin metamaterial absorber with polarization-selective resonant absorption at the prescribed wavelength. The metamaterial absorber with a configuration, "metasurface + grounded dielectric slab," provided unique possibility to design the pixels with different spectral and polarization sensitivity, using a single dielectric slab. The backside of the structure was covered with a high-performance infrared emissive layer. Absorption of terahertz

radiation led to heating of the structure and increasing IR emission in the emissive layer, which was henceforth detected by the IR camera. The matrix structure consisted of cells with different spectral and polarization sensitivity, which provided multispectral terahertz imaging with polarization discrimination in a real time regime. Such an imaging scheme provided high operational flexibility, making it a relatively simple but multifunctional solution for terahertz imaging.

ACKNOWLEDGMENT

The authors thank Nina I. Fedorinina and Evgeniy A. Lonshakov for sample preparation and Mikhail Astafiev for his assistance in measurements.

REFERENCES

1. Chang, C.-I, *Hyperspectral Imaging: Techniques for Spectral Detection and Classification*, Springer, 2003.
2. Chang, C.-I, *Hyperspectral Data Exploitation: Theory and Applications*, John Wiley & Sons, Inc., Hoboken, New Jersey, 2007.
3. Eismann, M. T., J. Kerekes, A. P. Schaum, and R. A. Leathers, "Multispectral and hyperspectral imaging: Introduction to the feature issue," *Appl. Opt.*, Vol. 47, MHI1–MHI1, 2008.
4. Adam, E., O. Mutanga, and D. Rugege, "Multispectral and hyperspectral remote sensing for identification and mapping of wetland vegetation: A review," *Wetlands Ecology and Management*, Vol. 18, 281–296, 2010.
5. Kruse, F. A., "Identification and mapping of minerals in drill core using hyperspectral image analysis of infrared reflectance spectra," *International Journal of Remote Sensing*, Vol. 17, No. 9, 1623–1632, 1996.
6. Govender, M., K. Chetty, and H. Bulcock, "A review of hyperspectral remote sensing and its application in vegetation and water resource studies," *Water SA*, Vol. 33, No. 2, 145–151, 2007.
7. Klemas, V., "Remote sensing techniques for studying coastal ecosystems: An overview," *Journal of Coastal Research*, Vol. 27, No. 1, 2–17, 2011.
8. Lins, E. C., S. Pratavieira, W. T. Shigeyosi, M. Dutra-Correa, V. S. Bagnato, C. Kurachi, and L. G. Marcassa, "Assembly, calibration and application of a hyperspectral image system for biomedical imaging," *WC 2009, IFMBE Proceedings 25/II*,

O. Dössel and W. C. Schlegel (eds.), 697–700, 2009. Available: www.springerlink.com.

9. Lee, Y.-S., *Principles of Terahertz Science and Technology*, Springer Science+Business Media, LLC, New York, 2009.
10. Woolard, D. L., W. J. O. Jensen, R. J. Hwu, and M. S. Shur, "Terahertz science and technology for military and security applications," *Selected Topics in Electronics and Systems*, Vol. 46, World Scientific Publishing Co. Pte. Ltd., Singapore, 2007.
11. Dexheimer, S. L., *Terahertz Spectroscopy: Principles and Applications*, CRC Press, Taylor & Francis Group, Boca Raton, FL, USA, 2008.
12. TeraView Company, Available: http://www.teraview.com.
13. Federici, J. F., B. Schulkin, F. Huang, D. Gary, R. Barat, F. Oliveira, and D. Zimdars, "THz imaging and sensing for security applications — Explosives, weapons and drugs," *Semicond. Sci. Technol.*, Vol. 20, S266–S280, 2005.
14. Watanabe, Y., K. Kawase, T. Ikari, H. Ito, Y. Ishikawa, and H. Minamide, "Spatial pattern separation of chemicals and frequency — Independent components by terahertz spectroscopic imaging," *Applied Optics*, Vol. 42, 5744–5748, 2003.
15. Kawase, K., Y. Ogawa, and Y. Watanabe, "Component pattern analysis of chemicals using multispectral THz imaging system," *Proc. SPIE*, Vol. 5354, 63–70, 2004, doi:10.1117/12.528517.
16. Han, P. Y., G. C. Cho, and X.-C. Zhang, "Time-domain transillumination of biomedical tissue with terahertz pulses," *Opt. Letters*, Vol. 25, 242–244, 2000.
17. Löffler, T., T. Bauer, K. J. Siebert, H. G. Roskos, A. Fitzgerald, and S. Czasch, "Terahertz dark-field imaging of biomedical tissue," *Optics Express*, Vol. 9, No. 12, 616–621, 2001.
18. Siebert, K., T. Löffler, H. Quast, M. Thomson, T. Bauer, R. Leonhardt, S. Czasch, and H. G. Roskos, "All-optoelectronic CW THz imaging for biomedical applications," *Phys. Med. Bio.*, Vol. 47, No. 21, 3743–3748, 2002.
19. Woodward, R. M., B. Cole, V. P. Wallance, D. D. Arnone, R. Pye, E. H. Linfield, M. Pepper, and A. G. Davies, "Terahertz pulse imaging of in-vitro basal cell carcinoma samples," *Lasers and Electro-Optics, CLEO'01, Technical Digest*, Optical Society of America, Washington, DC, 329–330, 2001.
20. Arnone, D., C. Ciesla, and M. Pepper, "Terahertz imaging comes into view," *Issue April 2000 of Physics World*, 35–40, Institute of Physics and IOP Publishing Limited, 2000.

21. Silverberg, R. F., S. Ali, A. Bier, B. Campano, T. C. Chen, E. S. Cheng, D. A. Cottingham, T. M. Crawford, T. Downes, F. M. Finkbeiner, D. J. Fixsen, D. Logan, S. S. Meyer, C. O'Dell, T. Perera, E. H. Sharp, P. T. Timbie, and G. W. Wilson, "A bolometer array for the spectral energy distribution (SPEED) camera," *Nuclear Instruments and Methods in Physics Research A*, Vol. 520, 421–423, 2004.
22. Kuznetsov, S. A., A. G. Paulish, A. V. Gelfand, P. A. Lazorskiy, and V. N. Fedorinin, "Bolometric THz-to-IR converter for terahertz imaging," *Applied Physics Letters*, Vol. 99, 023501-3, 2011.
23. Balanis, C. A., *Modern Antenna Handbook*, Wiley, John Wiley & Sons, Inc., USA, 2008.
24. Liu, T. S., A. F. Starr, and W. J. Padilla, "Infrared spatial and frequency selective metamaterial with near-unity absorbance," *Phys. Rev. Lett.*, Vol. 104, 207403-4, 2010.
25. Padilla, W. and X. Liu, "Perfect electromagnetic absorbers from microwave to optical," *Optical Design & Engineering, SPIE Newsroom*, 1–3, 2010, doi:10.1117/2.1201009.003137.
26. Beruete, M., M. Sorolla, R. Marques, J. D. Baena, and M. J. Freire, "Resonance and cross-polarization effects in conventional and complementary split ring resonator periodic screens," *Electromagnetics*, Vol. 26, 247–260, 2006.
27. Capolino, F., *Theory and Phenomena of Metamaterials*, Series Handbook of Artificial Materials, Vol. 1, CRC Press, Taylor and Francis Group, USA, 2009.
28. Lin, S. S., K. M. Yemelyanov, E. N. Pugh, Jr., and N. Engheta, "Separation and contrast enhancement of overlapping cast shadow components using polarization," *Opt. Express*, Vol. 14, No. 16, 7099–7108, 2006.
29. Lin, S. S., K. M. Yemelyanov, E. N. Pugh, Jr., and N. Engheta, "Polarization- and specular-reflection-based, non-contact latent fingerprint imaging and lifting," *Journal of the Optical Society of America A*, Vol. 23, No. 9, 2137–2153, 2006.
30. Demos, S. G. and R. R. Alfano, "Optical polarization imaging," *Appl. Opt.*, Vol. 36, 150–155, 1997.
31. Xuan, J., U. Klimach, H. Zhao, Q. Chen, Y. Zou, and Y. Wang, "Improved diagnostics using polarization imaging and artificial neural networks," *International Journal of Biomedical Imaging*, Vol. 2007, Article ID 74143, 11 Pages, 2007, doi:10.1155/2007/74143.